COMPARISIONS OF GROUND PENETRATING RADAR RESULTS AT CHANG'E-3 AND CHANG'E-4 LANDING SITES. J. L. Lai[1], Y. Xu[1], X. P. Zhang[1], L. Xiao[1,2], Q. Yan[1], X. Meng[1], B. Zhou[3], Z. H. Dong[3], and D. Zhao[3]
[1]State Key Laboratory of Lunar and Planetary Sciences, Macau University of Science and Technology, Macau (yixu@must.edu.mo) , [2]Planetary Science Institute, School of Earth Sciences, China University of Geosciences, Wuhan, China, [3]Key Laboratory of Electromagnetic Radiation and Detection Technology, Institute of Electronics, Chinese Academy of Science, Beijing, China.

Introduction: On 14 December 2013, Chang'e-3 (CE-3) landed at 340.49°E, 44.12°N in northern Mare Imbrium and released the Yutu rover. On 3 January 2019, Chang'e-4 (CE-4) landed at 177.588° E, 45.457° S (Statio Tianhe) in the Von Kármán crater of the SPA basin and released the Yutu-2 rover. The two rovers both equipped with ground-penetrating radars (hereafter referred to as Lunar Penetrating Radar, LPR) provide unique data sets of in situ measurements of the lunar regolith [1]. The aim of this work is to report the first five lunar days of CE-4 LPR results at 500 MHz and compare the results between the two sites.

Chang'e-3 and Chang'e-4 Landing sites

CE-3 probe landed in the Imbrium basin on basalts inferred as Eratosthenian in age. These represent some of the youngest units on the Moon at about 2.35-2.5 billion years (Gy) old[2], for instance compared with samples returned by the Apollo and Luna missions. Estimations of mafic components range from TiO_2 = 5 ± 1 weight percent (wt %) and FeO = 20 ± 2 wt % (derived from the gamma-ray spectrometer data onboard Lunar Prospector [3]) and TiO_2 = 4.0 wt % and FeO = 20.7 wt % (data from the Active Particle X-ray Spectrometer (APXS) instruments on the Chang'e-3 rover[4]. The titanium dioxide abundance of the geological unit Im1, ~15 km to the north, is lower at ~1.4 wt.%, also suggested by the low albedo (see Figure 1(a). The Yutu rover surveyed in total about a 114-meter-long track within the continuous ejecta deposits of the ~450-m sized Ziwei crater.

At the time of writing, the CE-4 Yutu-2 rover has travelled almost 200 m within the Von Kármán crater lying in the northwestern of the SPA basin, as shown in Figure 1(b)(c). The Von Kármán crater formed in the pre-Nectarian era and it was infilled with mare basalts during the Imbrian period. Subsequently, countless impact events both within and from outside the area infilled the crater with ejecta [5]. The absolute model age for the floor of Von Kármán crater was estimated as $3.6^{+0.09}_{-0.2}$ Ga based on crater size-frequency distribution measurements[5]. The surface materials have lower FeO contents (12–14 wt%) and the subsurface deposits have higher FeO contents (17–18 wt%) excavated by fresh craters.

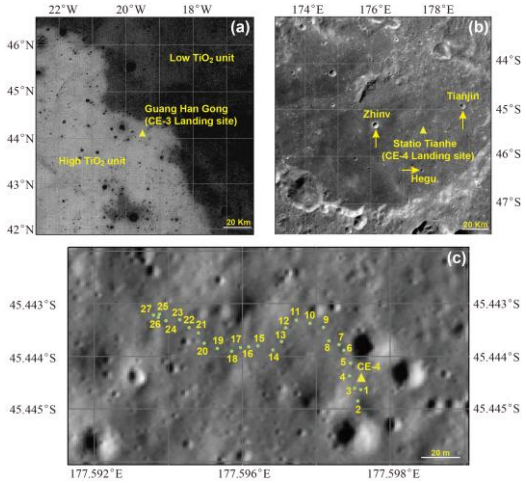

Figure 1 (a) The CE-3 landing site on TiO_2 map derived from Lunar Reconnaissance Orbiter Camera (LROC) Wide-Angle Camera (WAC) images (Sato et al., 2017). The bright color indicates high titanium area. (b) The CE-4 landing site on CE-2 Digital Orthophoto Map (DOM) with a resolution of 7 m/pixel. (c) The motion path of Yutu-2 rover. The base image was taken by the Lunar Reconnaissance Orbiter (LRO) Narrow Angle Camera (NAC) Camera.

Data: The LPR transmits a pulsed radar signal and receives the reflected signal along the rover traverse path. It operates at two channels with center frequencies at 60 MHz and 500MHz. The channel two has one transmitting and two receiving bow-tie shaped antennas deployed on the bottom board of the rover. The bandwidth of channel two is 450 MHz, corresponding to range resolutions of 0.3 m in the vacuum (Fang et al., 2014). The radar data of channel two collected along the 114 m (CE-3) and ~176 m (CE-4) long paths have been compared in this work.

Results:

Penetrating Depth. The penetration depth of the CE-3 is 131.0~176.5ns in terms of round-way transmission time. The CE-4 LPR can reach deeper up to 426.0~449.7ns, 2.85 times the detection limit of the CE-3 LPR. The detection ability of the LPR is closely related to tanδ, considering that the CE-3 and the CE-4 LPRs share the same set of radar parameters. The tanδ value at two landing sites can be estimated with FeO and TiO_2 abundances derived from the APXS experi-

ment[4] and the Kaguya Multiband Imager (MI) data. The different loss tangent values and non-neglectable geometric spread produces the 2.1~2.4-time difference in the detection depths between the two sites, close to the observations of the LPR results. One factor contributing further to the increase of the penetration depth at CE-4 site could be the lower abundance of near-surface large rocks than at the CE-3 site. The scattering from rocks increases the attenuations of the radar signal. Moreover, the thin fine-grained regolith layer at CE-3 site results in the LPR signals to decay rapidly in the underlying coarse-grained and blocky megaregolith layer, e.g. tanδ of Apllo17 site at the depth of 8 m can reach 0.08±0.04 [6], which may also explain the large difference of penetration depths at CE-3 and CE-4.:

Permittivity, bulk density and loss tangent. Figure 2(a) shows the comparisons between the average value of the real part of permittivity at CE-3 and CE-4 sites using the hyperbola method used in [7]. At the CE-4 site, $\bar{\varepsilon}$ increases slightly with depth and reaches 4.3 at 130 ns, while that of CE-3 is 3.5 of the top 40 ns (in terms of round-way delay) and then changes abruptly to 6 in the underlying layer, suggesting that the fine-grained lunar regolith layer at the CE-4 site is probably much thicker than at the CE-3 site given the permittivity of Apollo rock samples is 6-14[6].

The instantaneous permittivity profile of CE-4 is shown in Figure 2(b). It increases very rapidly at the near-surface section of the regolith (< 2 m) and then grows slowly to the maximum value of about 4.5 at the depth of 11 m. a bulk density for the regolith at CE-4 of ρ=1.22-2.23 g/cm^3 , increasing with depth as shown in Figure 2(c). This trend is comparable to observations at the Apollo sites and the estimated bulk density is in the higher end of the range measured from the Luna and Apollo samples, similar to that of Apollo 17 samples, which is 1.57 – 2.29 g/cm^3.

Figure 2(d) shows the estimated tanδ results of the R^2 correction along with the traversing path of the Yutu-2 rover between 0 and 105 m. The average value of $\tan\delta$ is 0.0039 ± 0.0002, in the lower range of laboratory measurement results of lunar soil samples[6], and agrees with the estimated results. The agreement shows that the LPR signal attenuation can be explained by absorption from the lunar regolith, the same as observed by the 1-16 MHz Surface Electrical Properties Experiment at the Apollo 17 site [8]. The implication of these two results is that heterogeneity on scales of 30 cm (wavelength of LPR in regolith) to 10 m is insufficient to significantly scatter electromagnetic waves. The FeO + TiO_2 content of the lunar regolith can be inferred as 11.8 - 13% at CE-4, which is consistent with 11-19% estimated with remote sensing data.

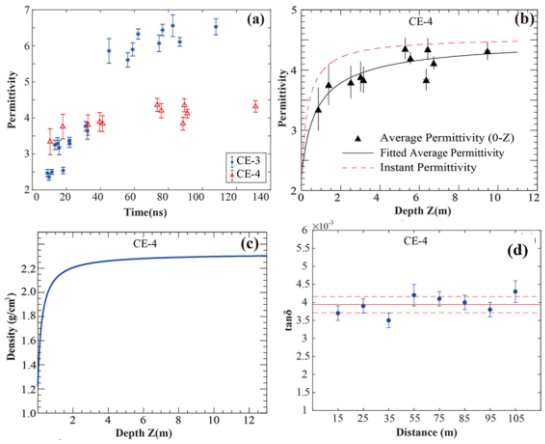

Figure 2 (a) Average permittivity value vs. two-way delay at the CE-3 and the CE-4 sites. (b) The depth profile of the fitted average permittivity and instantaneous permittivity at the CE-4 site. (c) The derived density-depth curve at the CE-4 site. (d)) The tanδ along the rover path.

Based on the derived permittivity, a piecewise function $\bar{\varepsilon} = 4.3\ (\tau \leq 154\ ns), \bar{\varepsilon} = 6\ (\tau > 154 ns)$ is used to carry out the time-to-depth conversion in radargram, which gives an estimate for the thickness of fine-grained lunar regolith at the CE-4 location of 11.1 ± 0.4 m.

Acknowledgments: This study was supported by the Science and Technology Development Fund (FDCT) of Macau (Grants 0042/2018/A2, 121/2017/A3, and 0089/2018/A3). Chang'e-3 (CE-3) Lunar Penetrating Radar (LPR) data, Panorama Camera images, and CE-2 Digital Orthophoto Map (DOM) are available at http://moon.bao.ac.cn. The Lunar Reconnaissance Orbiter Wide Angle Camera image for deriving TiO_2 map and Lunar Reconnaissance Orbiter (LRO) Narrow Angle Camera (NAC) image is available at http://wms.lroc.asu.edu/lroc.

References: [1] G. Y. Fang, et al. (2014) Res. Astron. Astrophys. 14, 1607. [2] J. Zhao, et al., (2014) Physics, Mech. Astron. 57, 569. [3] T. H. Prettyman, et al., (2006) JGR 111.[4] X. Zhang et al., (2015), EGU, Id. 726 17. [5] J. Huang, et al., (2018), JGR, 123, 1684. [6] W.D. Carrier, et al., (1991) Lunar source Book. [7] J. Lai, et al., (2016) Planet. Space Sci. 120, 96. [8] R. E. Grimm, (2018), Icarus 314, 389.